JOURNAL OF MATERIALS SCIENCE 18 (1983) 195–207

Mössbauer, EXAFS, and X-ray diffraction study of Fe^{3+} clusters in MgO:Fe and magnesiowüstite $(Mg,Fe)_{1-x}O$ – evidence for specific cluster geometries

GLENN A. WAYCHUNAS
Center for Materials Research, Stanford University, Stanford, California 94305, USA

Mössbauer and EXAFS analysis of Fe^{3+}-doped MgO rapidly quenched from 1200° C have yielded octahedral/tetrahedral Fe^{3+} site occupancy ratios which are used to place constraints on the possible defect cluster geometries. The data suggest the samples contain a range of defect aggregates consisting of combinations of basic dimer and trimer units (octahedral Fe^{3+} ions coupled to 1 or 2 cation vacancies) and variations about the "4–1" cluster motif. (Four cation vacancies surrounding one interstitial Fe^{3+}.) The groupings are consistent with lattice-energy calculations for defect clusters in both FeO and MgO, the observed sample colour, and prior TEM and ED observations of defect ordering in quenched wüstite. Low-temperature annealing of the samples results in cluster growth and changes in the Mössbauer spectrum attributable to production of magnesioferrite-like aggregates. The colour of the samples after annealing is indicative of grouping of magnetically interactive octahedral Fe^{3+} ions such as would be present in spinel nuclei. X-ray diffraction structure factor measurements of magnesiowüstite with 70 cation % Fe/(Fe + Mg) yield defect-concentration ratios similar to those observed in MgO and wüstite. This indicates that initial clustering of Fe^{3+} ions and cation vacancies probably results in similar structures throughout the MgO–FeO–Fe_2O_3 system.

1. Introduction

Although many studies have focused on the environment of Fe^{3+} in quenched MgO, few have been able to discern any definite cluster types or geometries except in low concentration (< 1000 ppm Fe^{3+}) samples. In these cases, dimer and trimer units (one cation vacancy with one or two adjacent octahedral Fe^{3+} ions) along ⟨1 0 0⟩ and ⟨1 1 0⟩ directions are thought to be the dominant species [1–6]. In samples with greater concentrations of Fe^{3+} in MgO or magnesiowüstite, no direct details of the clustering have been obtained, although it is known that larger clusters with varying degrees of magnetic behaviour form [4] and lattice-energy calculations suggest cluster motifs similar to those postulated for wüstite [5, 7].

Mössbauer spectroscopy of Fe^{3+} in MgO is perhaps the most obvious means of characterizing the Fe^{3+} cluster species. However, the analysis of dilute Fe^{3+} materials is often complicated by the onset of paramagnetic relaxation at low Fe^{3+} concentrations and the transition to a magnetic hyperfine spectrum at Fe^{3+} concentration levels where substantial clusters or precipitates exist. The technique is then best applied to the compositional range where small clusters are likely. These will behave paramagnetically, or superparamagnetically, and will give rise to Mössbauer parameters comparable to Fe^{3+} in other oxides and related compounds.

However, previous Mössbauer investigations [1, 2] have not attempted to interpret the complete absorption spectrum in terms of Fe^{3+} in substitutional (octahedral) and interstitial (tetrahedral) sites. The octahedral to tetrahedral (O/T) Fe^{3+} ratio is a function of cluster geometry and size,

0022–2461/83/010195–13$04.06/0

and hence can serve to identify cluster motif if local charge balance is maintained and it can be assumed that all Mg^{2+} and Fe^{2+} reside only on octahedral sites. Gonser *et al.* [1] reported only a single doublet absorption spectrum, which was attributed to octahedral Fe^{3+} with a nearby charge-compensating cation vacancy. Comparison of the observed quadrupole splitting (QS) with calculations based on a simple electrostatic model, suggested that a ⟨110⟩ orientation of the cation vacancy–Fe^{3+} unit was occurring. However, no spectral variations were reported over the composition range 0.05 to 6.5 cation % Fe^{3+} despite present evidence [4, 5, 7, 8] that cluster size and geometry is dependent on Fe^{3+} concentration in this range. Leider and Pipkorn [2] observed a more complex spectrum for 0.04 cation % Fe^{3+} in an MgO single crystal but did not attempt a complete structural interpretation.

The spectra described in this work are similar to that of Leider and Pipkorn; however, a quantitative fit of Fe^{3+} octahedral and tetrahedral concentrations has been made by assigning spectral features according to the constraints of known Fe^{3+} Mössbauer parameters, and EXAFS determinations of relative Fe^{3+} site occupancies. In order to enhance the quality of recorded spectra, several of the samples used in the investigation were enriched in ^{57}Fe. Additionally, quench was performed as rapidly as possible (500 to 1000° C sec^{-1}) from 1200° C to reduce decomposition.

Comparison of the results with an X-ray diffraction study of site occupation on 70% Fe magnesiowüstite and related data for magnesiowüstite and wüstite in the literature suggests that clustering over the entire $MgO–FeO–Fe_2O_3$ system is similar, and that the formation of spinel during quench proceeds by the growth of spinel-like units from non-spinel-like original clusters. Changes in the Mössbauer spectrum and physical coloration of the samples upon low-temperature annealing are consistent with growth of spinel clusters and variation of the O/T Fe^{3+} ratio towards that in bulk magnesioferrite.

2. Experimental procedure

2.1. Sample preparation

1/2, 1 and 2 cation % Fe starting mixes consisting of very fine crystals of MgO and $MgFe_2O_4$ were prepared by a freeze-dry process [8, 9] to ensure maximum homogeneity and reactivity. 90%-enriched ^{57}Fe was used to enhance Mössbauer absorption in the 1/2 and 1 cation % mixes. The MgO : Fe^{3+} samples were synthesized in a quench furnace described by Waychunas [8]. The mixes were loaded into 0.5 cm diameter Pt tubing 1 cm long, which was then crimped, closed, and flattened to maximize the contact between Pt and sample. A Pt wire held the charges in the hot spot of the furnace during synthesis, after which they were released into a cold-water bath. A weight attached to each charge assured a speedy and reproducible quench. Calculations indicated that the Pt tube cooled to 100° C within about 200 msec after striking the water.

The synthesis anneal was of 2 to 4 h duration at approximately 1200° C with an air atmosphere. Subsequent lower temperature anneals were carried out in a muffle furnace. The higher Fe concentration magnesiowüstite samples were prepared at 1080° C over 12 to 24 h as thin discs of 1.26 cm diameter to produce sufficient material for X-ray and Mössbauer analysis. These samples were similarly quenched. Thermogravimetric analysis was used to determine Fe^{3+} concentration [8].

2.2. Mössbauer spectroscopy

The Mössbauer spectra were recorded on a TRACOR-NORTHERN Econ-1A 1024 channel analyser, which furnished timing signals to synchronize a Kankeleit [10] type electronic drive-electromechanical transducer for collection of a constant acceleration spectrum (linear velocity increment with channel number). 512 memory channels were used for low velocity ranges, approximately 3.8 to $-3.8\,mm\,sec^{-1}$ for the spectra considered here. Only the first half of the two mirror-image spectra data set was analysed.

Velocity calibration of the spectrometer was accomplished by fitting observed velocities of well-documented standard absorption lines to a second or third polynomial curve as a function of channel number. Spectrometer drift between spectra was estimated at less than $0.02\,mm\,sec^{-1}$ at any given channel.

The source material for all experiments was ^{57}Co in a Pd matrix as supplied by New England Nuclear. The initial quantity of ^{57}Co was 10 to 15 mCi.

The spectrometer was operated in the moving source mode, with the detector to source distance varying about 0.1 cm during operation. This created background intensity variation of 0.2% which was corrected by the spectral fitting pro-

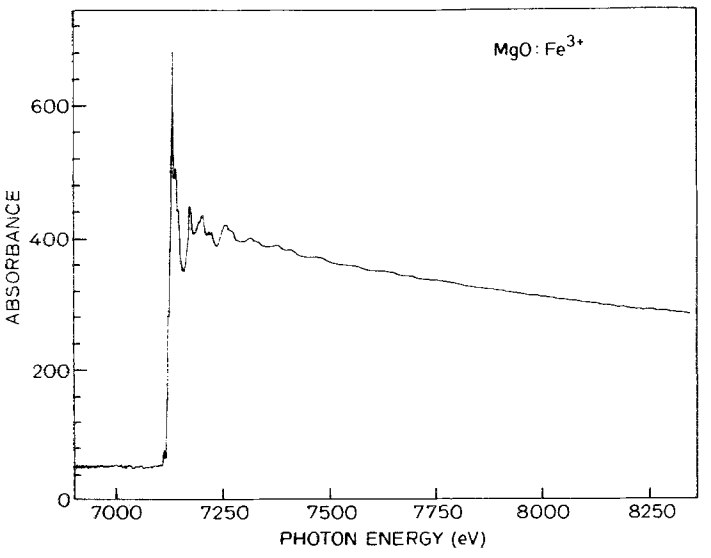

Figure 1 Raw K-edge absorption spectrum of Fe^{3+}-doped MgO. The spectrum is an average of four individual scans.

gramme. All samples were finely ground and placed in polyethylene vial lids in amounts necessary to achieve a ^{57}Fe density of 0.1 to 0.2 mg cm^{-2}. Vaseline was used as a binder. At least 10^6 counts per channel were collected in all cases. Isomer shifts (IS) are quoted here with reference to the source, ^{57}Fe in Pd. To convert to isomer shifts relative to ^{57}Fe in Fe metal, add 0.177 mm sec^{-1} to the values given.

2.3. *K*-edge and EXAFS data collection and analysis

Fe *K*-edge and EXAFS spectra were collected at the Stanford Synchrotron Radiation Laboratory (SSRL) during non-dedicated storage ring operation. Beam line 1-5 was utilized with a (220) channel out silicon crystal monochromator. Energy resolution was better than 0.7 eV. In order to obtain a sufficiently strong Fe absorption signal, samples MW-59 and MW-61 were combined. Test spectra indicated negligible effect from any Fe in the Be windows of the monochromator system vacuum-line port. Spectral scans from 6900 to 7950 eV required 20 min. A thin Fe foil standard supplied by SSRL was used to calibrate the energy of the monochromatized beam. The first inflection point in the Fe *K*-edge spectrum was taken as 7111.3 eV. Energy drift was found to be less than 0.1 eV during the collection period (2.5 h). Details of the experimental apparatus on beam line 1-5 are described by Hunter [11].

2.4. EXAFS analysis

The analysis procedure for EXAFS spectra has been described in detail by Brown and Doniach [12]. The raw average of four spectra of Fe^{3+}-doped MgO is shown in Fig. 1. The absorption background curve is fitted with a multiregion cubic spline function far from the major EXAFS wiggles and extrapolated to the *K*-edge and then subtracted yielding the EXAFS absorption alone. This is converted from energy into momentum units prior to Fourier transformation. The EXAFS amplitude weighted by the factor K^2 is plotted versus the momentum of the backscattered wave in Fig. 2. The zero energy for the wave vector, E_0, was taken as 7130 eV.

Fourier transformation over the region $0.35 < k < 1.45$ nm yields the modified radial distribution function (RDF) depicted in Fig. 3. Owing to the phase shift of the backscattered wave produced during the absorption process, the R values in the RDF are shifted from the actual values by a fraction of an Ångstrom. This shift in R can be obtained independently from analysis of compounds of known interatomic spacings which have the same absorber-scatterer pair and are transformed over identical ranges in k. For the present study Fe^{2+}-doped MgO and Fe^{3+} in γ-$LiAlO_2$ and α-$LiFeO_2$ were surveyed as model compounds.

The first shell region of the RDF, that between 0.1 and 0.21 nm in Fig. 3 and representing only Fe nearest-neighbour backscatterers, was back transformed for detailed analysis. This Fourier-filtered EXAFS was then fit with a model EXAFS function where the number of oxygen neighbours and their distances were variables (Fig. 4).

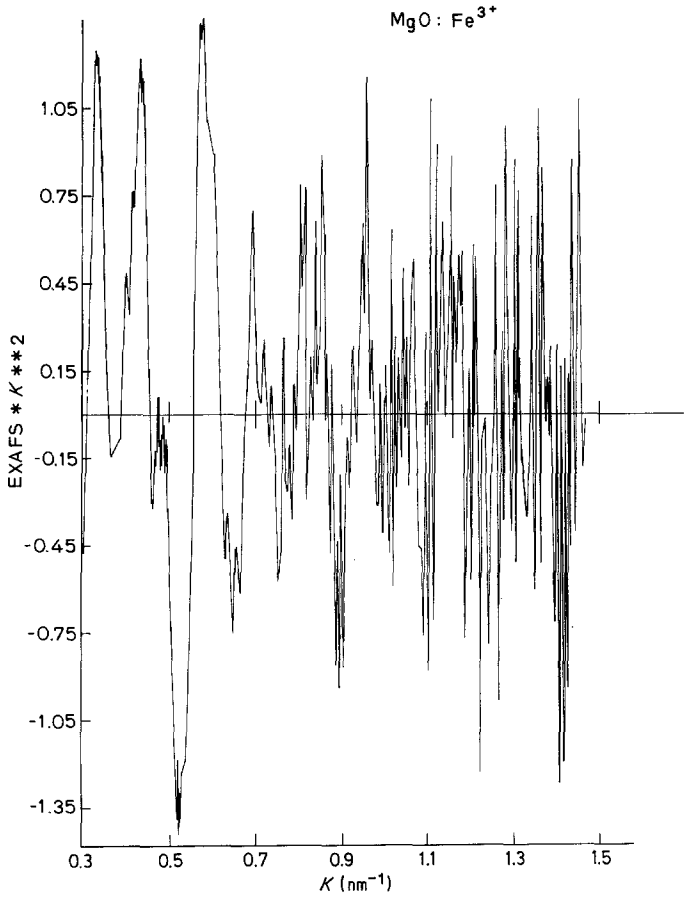

Figure 2 The EXAFS oscillations separated from the raw absorption spectrum. The abcissa is the momentum of the scattered wave vector, and the ordinate is a normalized intensity multipled by K^2. This factor is necessary because of a tendency of the amplitude of the EXAFS oscillations to dampen out exponentially with increasing K.

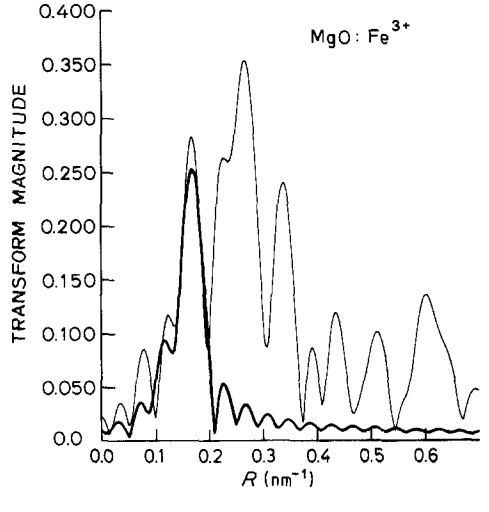

Figure 3 The pair correlation function produced by direct Fourier transformation of the data from Fig. 2. The function is similar to a radial distribution function except that only absorber-scatterer pair correlation functions make any contribution. The bold curve is a Fourier filtered function obtained from the fitted EXAFS oscillations of Fig. 4.

3. Results

3.1. EXAFS

Fig. 4 depicts two model fits to the first shell EXAFS oscillations of Fe^{3+} in MgO. In the first trial a single ligand distance was constrained, resulting in a Fe^{3+}–O bond length of 0.199 nm with 3.9 oxygen neighbours. χ^2 for this fit was 0.6563. Fitting with two distances resulted in a significant improvement, reducing χ^2 to 0.2828 and yielding the values:

5.5 Fe–O bonds at 0.201 nm

1.9 Fe–O bonds at 0.183 nm.

Fits using three or more distances tended to converge to these two sets of values. Since the distances derived from the EXAFS data depend only on the phase of the K-space oscillations and not on their amplitudes, it is possible to directly compare the distances above with those for model compounds of known structure analysed in analogous fashion. This comparison suggests an

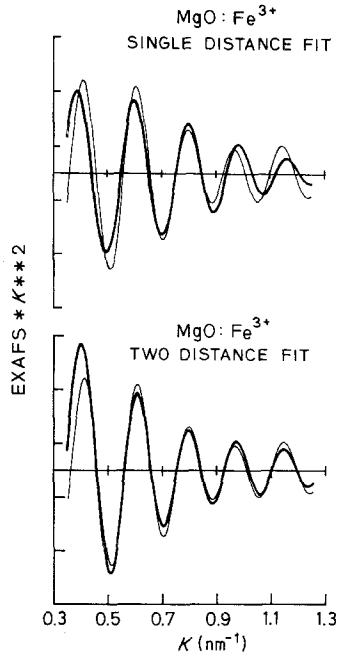

Figure 4 Comparison of two fits to Fourier-filtered EXAFS oscillations. The light curves are the back Fourier transformed oscillations from the correlation function of Fig. 3 over the first-neighbour distance shell (1 to 2.1 Å) The heavy curves indicate two calculated model EXAFS functions. The better fit involving two Fe–O distances was retransformed to produce the Fourier filtered first shell peak of Fig. 3.

uncertainty in the bond distances of ± 0.002 nm. The RDF from the best-fit first-shell EXAFS is plotted as the bold line in Fig. 3.

In general, EXAFS-derived coordination numbers are not more accurate than about 20%, even in favourable cases [13, 14]. However, owing to the strong correlation of Fe^{3+}–O bond length with Fe^{3+} coordination number [15, 16], the 0.201 and 0.183 nm distances can be readily attributed to octahedral and tetrahedral environments, respectively. Given this assignment, the EXAFS-fit coordination numbers can be recast according to the number of observed Fe^{3+}–O bonds, i.e., 74% are 0.201 nm, 26% are 0.183 nm. If the actual coordination numbers are restricted to only 4 and 6, respectively, then the ratio of Fe^{3+} sites is: 0.74/6 : 0.26/4, or 66% octahedral and 34% tetrahedral. Because thermal vibrational amplitude affects EXAFS amplitudes [11], it is expected that the larger octahedral site may be somewhat underrepresented. The presence of about 9% Fe^{2+}/total Fe (derived from Mössbauer line areas) in the sample represents too small an amplitude contribution to the EXAFS spectrum to fit accurately.

3.2. Fe *K*-edge structure

The Fe *K*-edge contains structures due to several bound state electronic transitions. The lowest energy of these, the 1s → 3d absorption, is known to vary in intensity as a function of absorber site geometry. In tetrahedral Fe^{3+} spectra, for example, the 1s → 3d line may be about seven times more intense than it would be in spectra of octahedral Fe^{3+} species [17]. It has also been found that the intensity of this transition increases with site distortion in octahedral Fe^{3+} compounds [18]. α-$LiFeO_2$ has moderately distorted octahedral Fe^{3+} sites, and its Mössbauer spectrum is a wide doublet with QS similar to that observed for octahedral Fe^{3+} in MgO. Its relative 1s → 3d intensity is, therefore, expected to be similar to that for octahedral Fe^{3+} in MgO. A comparison of the background-corrected 1s → 3d line-intensity between α-$LiFeO_2$ and Fe^{3+}-doped MgO revealed about an 80% larger intensity in the MgO : Fe^{3+} samples. This is consistent with a substantial concentration of tetrahedral Fe^{3+} in this material. However, the uncertainties involved in the measurement of the low intensity 1s → 3d line (1 to 3% of total *K*-edge absorption) and the lack of suitable standards preclude accurate calculation of tetrahedral Fe^{3+} occupancy by this method. The best estimate, assuming seven-fold intensity enhancement for tetrahedral Fe^{3+} and octahedral Fe^{3+} intensity equal to Fe^{3+} in α-$LiFeO_2$ intensity, is about 15% tetrahedral/total Fe^{3+}. If the intensity from octahedral Fe^{3+} in MgO is less than from Fe^{3+} in α-$LiFeO_2$, then the proportion of tetrahedral Fe^{3+} could be larger and closer to the EXAFS estimates.

3.3. Mössbauer spectra

The Mössbauer spectra of samples MW-59 and MW-61 were fitted with two 95% Lorentzian–5% Gaussian doublets and a singlet representing two ferric and one ferrous species, respectively. Although constraints on line positions or areas were necessary to achieve convergence initially, final refinement of the least squares fit could be performed with only the minimal constraint of equal line width and area for the two halves of a given doublet. The fitted spectra appear in Fig. 5.

At these low Fe^{3+} concentrations, paramagnetic relaxation must be considered [19]. However,

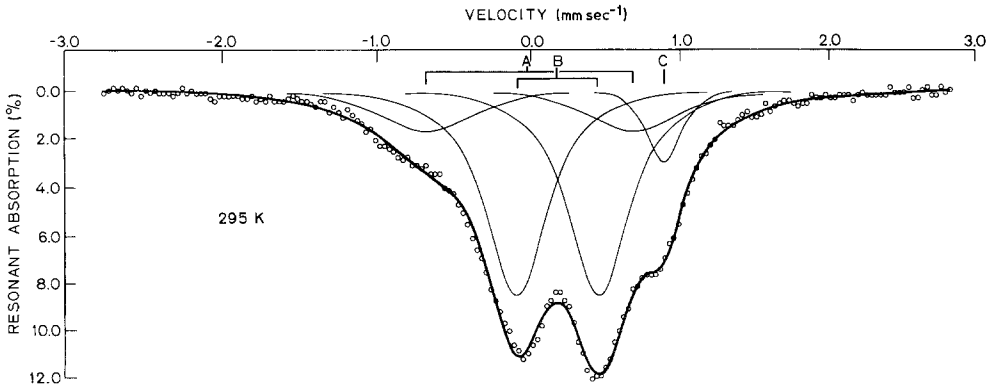

Figure 5 Representative Mössbauer spectrum of Fe^{3+}-doped MgO quenched from 1200° C. The A and B doublets refer to tetrahedral and octahedral Fe^{3+}, respectively. The C singlet represents octahedral Fe^{2+}. The solid lines are all computer fits to the observed absorption envelope which has been indicated by circles.

examination of the shape of the Mössbauer absorption, both in room and liquid-nitrogen temperature spectra, showed in neither case any extreme line broadening or increased doublet asymmetry, rendering it unlikely that paramagnetic relaxation was occurring. Similarly, a check was made of the Doppler velocities where ferrimagnetic bulk magnesioferrite peaks would be expected. No evidence for ferrimagnetic $MgFe_2O_4$ was observed in any of the spectra of Fe^{3+} in MgO prepared in air at 1200° C or under reducing conditions at 1080° C and rapidly quenched. X-ray diffractometer scans verified the absence of a spinel phase in the low Fe^{3+} samples. However, given the probably extreme diffraction line broadening expected for very small (less than 5.0 nm) particles, this method is probably too insensitive for adequate detection of spinel in low Fe samples.

The Mössbauer spectral fit parameters for the two high-temperature samples were consistent with the EXAFS results and the ferric site assignments (Table I). The IS for the higher velocity doublet was 0.18 ± 0.01 mm sec^{-1}, in agreement with a large body of Fe^{3+} spinel and oxide data for octrahedral occupancy. The IS for the lower velocity doublet was 0.00 ± 0.02 mm sec^{-1}, in agreement with much oxide and silicate data for tetrahedral Fe^{3+}, but considerably lower than the IS of tetrahedral Fe^{3+} in $MgFe_2O_4$ given by Degrave *et al.* [20] of 0.09 ± 0.01 mm sec^{-1}. This is reasonable, however, since the IS is known to decrease with decreasing first-neighbour atom distances, and the EXAFS-derived tetrahedral distance is smaller than the bond lengths in $MgFe_2O_4$ (0.192 nm) but similar to those in silicates. The QS of the octahedral doublet was 0.54 ± 0.01 mm sec^{-1}, while that of the Fe^{3+} tetrahedral doublet was 1.33 ± 0.02 mm sec^{-1}. The latter value is moderately large for a ferric absorption and suggests considerable distortion of the tetrahedral site or nearby structure from cubic symmetry. The line widths of the octahedral Fe^{3+} doublet are about 50% larger than in analogous single Fe^{3+} site compounds suggesting a range of octahedral environments. The line width of the tetrahedral Fe^{3+} doublet was about twice the expected single site width, suggesting an even larger range of local environments. On the basis of absorption line area ratio, the proportion of Fe^{3+} in tetrahedral coordination in samples MW-59 and MW-61 is $24 \pm 1\%$ and $27 \pm 1\%$, respectively. The average of 25.5% compares well with the 34% obtained from the EXAFS fitting considering the uncertainties in the EXAFS amplitudes. Also, the Mössbauer-derived site occupancies are roughly consistent with the intensity of the $1s \rightarrow 3d$ *K*-edge absorption feature.

A small recoil-free fraction dependence on coordination number and temperature [21] may slightly enhance the observed Mössbauer tetrahedral occupancy by a factor of about 1.06 at room temperature. However, no significant change in tetrahedral doublet line area was noticed in liquid-nitrogen temperature spectra, indicating that any recoil-free fraction variation between the two temperatures was smaller than the uncertainties in the fitting procedure.

The singlets fitted to the Fe^{2+} absorption are all at an IS position expectable for octahedral Fe^{2+} in oxides (0.87 mm sec^{-1}) and have widths as small as the best crystalline standard compounds. This is indicative of highly symmetrical Fe^{2+} sites

TABLE IA EXAFS fit results for Fe^{3+}-doped MgO (MW-59 + MW-61)

Fit region (nm^{-1})	Distances (nm)	Relative amplitudes (%)	Coordination corrected amplitudes (%)	χ^2
40–120	0.201	100	–	0.6563
40–120	0.201	74	66	0.2828
	0.183	26	34	

TABLE IB Mössbauer parameters for Fe^{3+}-doped MgO

Sample	MW-59	MW-61	MW-62	MW-64
Fe^{2+}: IS	0.86	0.88	0.88	0.81(5)
Γ	0.29	0.29	0.30	0.30
Area fraction	0.107(6)	0.075(4)	0.028	0.007
Fe^{3+}: Doublet 1: IS	0.170	0.180	0.175	0.175
QS	0.56	0.55	0.66	0.62
Γ	0.45	0.49	0.44	0.48
Area fraction	0.680(25)	0.675(22)	0.570(23)	0.487(30)
Fe^{2+}: Doublet 2: IS	−0.02	0.00	0.00	0.085
QS	1.33	1.36	0.89	1.03
Γ	0.74	0.81	0.63	0.66
Area fraction	0.213(24)	0.250(21)	0.402(21)	0.407(27)
Misfit	0.262%	0.143%	0.165%	0.067%
Δ Misfit	0.034%	0.014%	0.011%	0.007%

TABLE IC Sample compositions (cation %)

Sample	Fe^{2+}	Fe^{3+}	Mg
MW-59	0.22	1.78	98.0
MW-61	0.77	0.923	99.0
MW-62	≈ 0.01	≈ 0.99	99.0
MW-64	≈ 0.01	≈ 0.99	99.0

and suggests that there is probably little association of Fe^{3+} (particularly tetrahedral Fe^{3+}) and Fe^{2+} in the structure. High-spin Fe^{2+} is much more sensitive to small amounts of site distortion than is Fe^{3+} [22], and a non-zero QS would be expected if there were significant Fe^{3+}–Fe^{2+} pairing.

Numerous other fit models were also attempted on the spectra, including IS values constrained to those observed by Degrave *et al.* in $MgFe_2O_4$ (octahedral Fe^{3+} 0.18 mm sec^{-1}, tetrahedral Fe^{2+} 0.09 mm sec^{-1}), additional doublets, or an asymmetrical doublet. No plausible model resulted in statistically more significant fits than the unconstrained original trials as judged by Ruby's misfit parameter [23]. In fact, the Degrave *et al.* values produced substantially poorer fits, with considerable intensity left unfit at the low velocity end of the spectra.

3.4. Effect of second anneal at lower temperature

Portions of sample MW-61 were subjected to 900 and 500° C anneals in air for 1 h and 9 days, respectively, in an attempt to enhance Fe^{3+} clustering. While the original samples were yellow-green in colour, the re-annealed materials became orange in colour.

Fe^{3+} on tetrahedral sites in an oxide should produce a pale green coloration [24], and octahedral Fe^{3+} a very weak coloration if there is no Fe^{3+}–O^{2-}–Fe^{3+} interaction. However, clustering of Fe^{3+} with O^{2-} bridges, as would be created by adjacent Fe^{3+} ions in an MgO structure should produce strong coloration which increases with cluster size. This colour intensification has been studied in several mineral phases [25], and correlates with the onset of magnetic coupling between the Fe^{3+} ions in the structure. The coloration in these species is similar to that observed for the MgO: Fe^{3+} samples.

Despite the presumed growth of larger clusters and perhaps $MgFe_2O_4$ nuclei, no spinel phase was observed via X-ray diffractometry. Since the coloration observed was less intense than a mixture of $MgFe_2O_4$ and MgO of similar bulk composition, it appeared that either (1) little or no $MgFe_2O_4$ had formed or (2) any $MgFe_2O_4$ nuclei were extremely small.

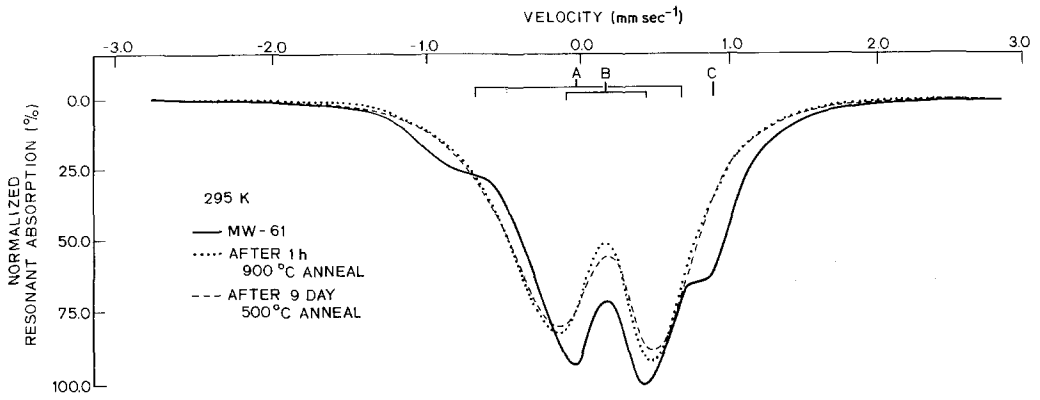

Figure 6 Comparison of the Mössbauer spectrum of annealed and as-quenched Fe^{3+}-doped MgO. Positions A, B and C have the same meaning as in Fig. 5 and refer to the computer-fitted line positions in the as-quenched spectrum (solid line). The other curves refer to annealed samples of the original quench material. Individual computer-fitted lines have been omitted for clarity.

Mössbauer spectra of the samples showed subtle, but significant, differences from the original high-temperature annealed and rapidly-quenched material, especially when attempts were made to apply the same fitting technique. In Fig. 6 the spectra of the samples annealed at the two temperatures are compared. Besides the loss of the Fe^{2+} peak, there are changes in the shape of the Fe^{3+} absorption. The minima have separated further and broadened and the low velocity "tail" has lost intensity. These changes are most likely due to site population and distortion variation among the Fe^{3+} species, or possibly to the onset of magnetic ordering.

By comparison with the Mössbauer spectra of $MgFe_2O_4$ [20] and α-Fe_2O_3 [26] over a wide temperature range, the onset of magnetic order should produce a dramatic broadening in the spectrum as the magnetic hyperfine lines appear, first at low average field (small splitting) and then moving toward their bulk $MgFe_2O_4$ line positions (large field, large splittings) as magnetization becomes complete. The effect of the small particle size and temperature are analogous: raising the temperature for a given particle size eventually removes the magnetic hyperfine pattern and induces a superparamagnetic spectrum. At a given temperature, reducing the particle size has the same effect. Apparently the particle sizes of $MgFe_2O_4$ or other Fe^{3+}-rich precipitates or clusters in the samples of this investigation are small enough to preclude magnetic hyperfine splitting, since no such features are evident either at room or liquid-nitrogen temperature. Furthermore, the absence of $MgFe_2O_4$ X-ray diffraction lines and the qualitative coloration are consistent with particle sizes below a unit cell in size. Units of this order of size should behave paramagnetically or superparamagnetically even at liquid-nitrogen temperatures.

3.5. Spectral fitting

The spectra of the 9-day 500° C and 1-h 900° C samples were alike except for a slightly greater broadening in the longer anneal sample evident by the smaller rise between the principal absorption minima. Fits of these spectra were less quantitative than the fits of MW-59 and MW-61 owing to the high correlation of fitted doublet and singlet line parameters. It was possible to generate equally good fits for several different models because of this. In general, however, statistically good fits required a tetrahedral Fe^{3+} doublet with some combination of reduced IS and QS and an increased area fraction of the total absorption compared to the fits of MW-59 and MW-61. This is consistent with a change in the Fe^{3+} site population in the direction of $MgFe_2O_4$ wherein about 40% of the Fe^{3+} resides on tetrahedral sites [27, 28]. Representative parameters for the fits appear in Table I.

3.6. Fe^{3+} site occupancy in high Fe magnesiowüstite from X-ray powder diffraction structure factor calculations

Corrected integrated intensities from ten Bragg reflections of seven magnesiowüstite powder samples with $Fe/(Fe + Mg) = 0.7$ and varying Fe^{3+} content were compared with intensities

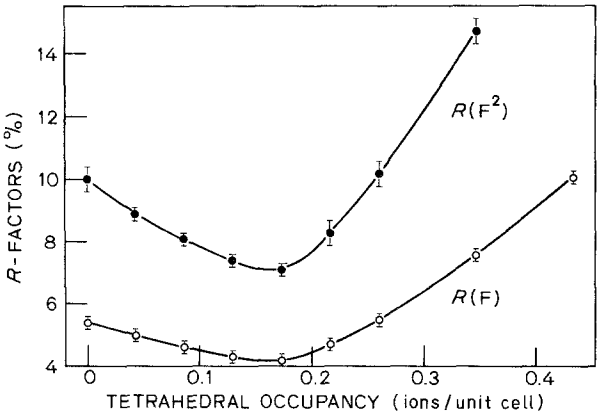

Figure 7 Example of $R(F^2)$ and $R(F)$ curves for magnesiowüstite sample MW-35. The minimum represents best agreement of calculated and observed structure factors.

calculated from a theoretical magnesiowüstite solid whose Fe/(Fe + Mg) and Fe^{3+}/total Fe ratios were constrained, but whose ferric iron distribution could be adjusted between octahedral and tetrahedral sites. Residual functions $R(F)$ and $R(F^2)$ were calculated as a function of tetrahedral occupancy. An example of the resulting curves, which were approximately parabolic in form and of varying curvature, is illustrated in Fig. 7. The average estimated error in the observed intensities was applied graphically to the curves to yield an uncertainty in the tetrahedral occupancy. The values obtained and their errors are plotted in Fig. 8 as a function of Fe^{3+}/total Fe and tabulated in Table II. Although the errors in the tetrahedral occupancy are large, and one sample produced anomalous results probably due to an incorrect Fe^{3+} analysis used in the structure factor calculation, it seems clear that a tetrahedral occupancy of 25 ± 7% is supported by the data. Similar measurements were also attempted on 30% Fe magnesiowüstite. However, these were unsuccessful owing to the correspondingly smaller overall tetrahedral occupancy in the samples.

4. Discussion

4.1. Defect arrangement in MgO: Fe^{3+} and magnesiowüstite

The Mössbauer, EXAFS, and K-edge results for MgO: Fe^{3+} suggest a proportion of tetrahedral Fe^{3+} which is 29 ± 5% of the total Fe^{3+}. The Mössbauer fits also suggest a relatively small concentration of isolated octahedral Fe^{3+} substituting for Mg^{2+}. If the proportion of tetrahedral

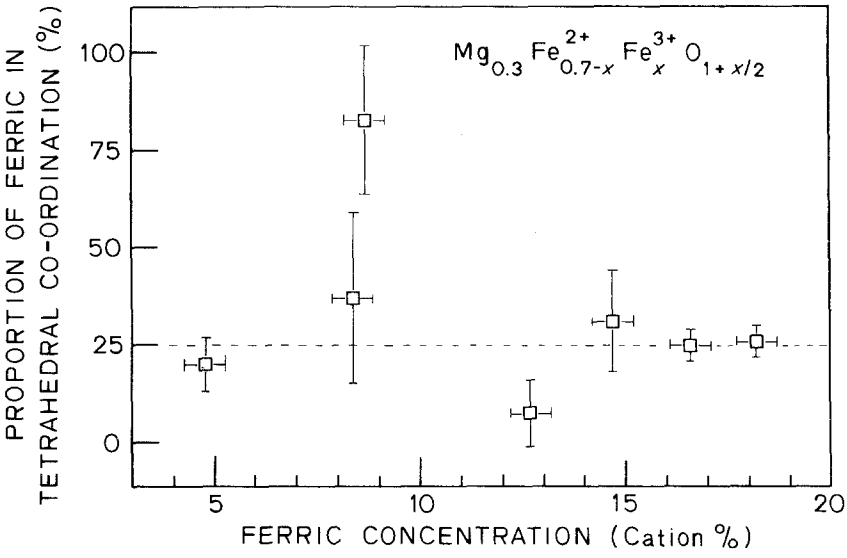

Figure 8 Tetrahedral Fe^{3+} occupancy in high Fe magnesiowüstite quenched from 1140° C as a function of Fe^{3+} concentration. The site occupation was adjusted in each case to minimize $R(F^2)$ calculated from powder X-ray diffraction structure factors. The error bars are explained in the text.

TABLE II Tetrahedral occupancy in 70% Fe magnesiowüstite

Sample	$Fe^{3+}/(Fe^{3+} + Fe^{2+} + Mg)$	Minimum $R(F)$	Minimum $R(F^2)$	Tetrahedral Fe^{3+}/Fe^{3+} total	σ
MW-26	0.048	0.027	–	0.20	0.068
MW-31	0.084	0.058	0.107	0.37	0.22
MW-33	0.087	0.061	–	0.82	0.17
MW-28	0.127	0.044	0.081	0.075	0.08
MW-27	0.147	0.055	0.111	0.31	0.13
MW-35	0.177	0.042	0.070	0.25	0.04
MW-36	0.182	0.027	0.069	0.26	0.04

species could be assumed to represent the motif of a single dominant type of defect cluster, then clusters of "6–2" and "8–3" type would be indicated. These consist of two or three "4–1" clusters, each comprised of four cation vacancies surrounding an interstitial Fe^{3+} ion, which share a common polyhedral edge and two of the vacancies. In order to achieve charge balance, it is necessary for six octahedral Fe^{3+} ions to reside near the "6–2" cluster, producing an O/T ratio of 3. Similarly, seven octahedral Fe^{3+} ions must be present near the "8–3" cluster, yielding an O/T ratio of 2.33. Since these charge-compensating Fe^{3+} ions can substitute for Mg^{2+} on any of a large number of cation sites around the cluster, a range of Mössbauer parameters for both the octahedral and tetrahedral Fe^{3+} is anticipated. This would result in broadened doublet lines, as have been observed.

Unfortunately, other cluster geometries can result in similar O/T ratios. For example, a "3–1" cluster, consisting of three cation vacancies and one tetrahedral Fe^{3+} with three nearby charge-compensating octahedral Fe^{3+} ions, has an O/T ratio of 3.0. Likewise, a unit of the inverse spinel structure with 25 cation vacancies and eight tetrahedral Fe^{3+} ions would have 26 octrahedral Fe^{3+} ions on average and an O/T ratio of about 3.25. This ratio decreases with increasing cluster size since charge-compensating octahedral Fe^{3+} ions at the cluster–host boundary make a proportionally smaller contribution to the O/T ratio approaching 1.0 for a perfectly inverse spinel and about 1.5 in the case of magnesioferrite. However, the lattice energy calculations noted above [5, 7] suggest that certain clusters are inherently more stable than others. In particular, the ⟨100⟩ oriented trimer and combinations of the basic 4–1 cluster unit, i.e., the 6–2, 8–3, "16–5" (subunit of the normal spinel structure) are the most stable geometries. The stabilities of larger spinel clusters were also found to increase with cluster size.

The apparent coloration of $MgO:Fe^{3+}$ is also an indication of cluster geometry, although qualitative. The pale yellow–green colour noted in the rapidly quenched samples is consistent with clusters containing a few magnetically interacting octahedral Fe^{3+} ions, but not with three or more [24]. Hence it is unlikely that many Fe^{3+} defect clusters in the MgO could have a large number of closely bound charge-compensating octahedral Fe^{3+}. Certainly the larger spinel-like clusters are disfavoured. A 4–1 cluster, for example, with five octahedral Fe^{3+} ions in some arrangement on the 24 nearest cation sites, should give rise to strong coloration if the Fe^{3+} ions tend to reside adjacent to cation vacancies.

Arrangements of Fe^{3+} ions which would produce minimal coloration are also possible, but for only these types to be represented requires a constancy of cluster motif inconsistent with the small energy differences among the possible motifs. Furthermore, the Mössbauer absorption lines would not be as broad as observed if only a few well-defined clusters were present.

In the case of 6–2 and 8–3 clusters, most octahedral Fe^{3+} arrangements around the cluster core would create several O^{2-} bridged Fe^{3+} and strong coloration. Hence the spectral and coloration observations require clusters smaller than 4–1 units, but with an average O/T ratio of about 2.4 to 3.0.

In situ equilibrium observations of 310 ppm Fe^{3+} in single crystal MgO [6] indicate that most Fe^{3+} at 1200° C resides on isolated octahedral sites. Dimers of one Fe^{3+} ion and a cation vacancy also occur, and increase in number during low-temperature anneal. This creates a reduction in the concentration of isolated cation vacancies. The kinetics of clustering appear to obey a second-order rate law during anneal, possibly due to the reaction of two dimers and an isolated octahedral Fe^{3+} to form a "3-cluster". At the concentration levels treated in the present work, it is likely that a

large population of dimers and dimer aggregates exists at equilibrium. Owing to the stability of the 4–1 configuration, it is probable that this geometry would be the next to develop during decomposition. Thus one possible picture of the quenched-in defect aggregation is a range of units representing the formation of 4–1 units from smaller clusters and isolated defects. The first steps would assemble dimers and isolated octahedral Fe^{3+} ions into trimers, tetramers, and "3-clusters". For example, using Kroger notation where $Fe \cdot Mg$ = octahedral Fe^{3+}, $V''Mg = Mg$ cation vacancy in MgO and $Fe_I^{\cdot\cdot\cdot} = Fe^{3+}$ interstitial in MgO, one may have:

$$Fe \cdot Mg + V''Mg \rightarrow Fe \cdot Mg\text{–}V''Mg \text{ (dimer)}$$

$$\text{dimer} + Fe \cdot Mg \rightarrow Fe \cdot Mg\text{–}V''Mg\text{–}Fe \cdot Mg \text{ (trimer)}$$

$$\text{trimer} + \text{dimer} \rightarrow Fe \cdot Mg\text{–}V''Mg\text{–}Fe \cdot Mg\text{–}V''Mg\text{–}Fe \cdot Mg \quad (\text{"3-cluster"})$$

$$\text{"3-cluster"} \rightarrow Fe \cdot Mg\text{–}V''Mg\text{–}Fe_I^{\cdot\cdot\cdot}\text{–}V''Mg\text{–}Fe \cdot Mg \quad (V''Mg \text{ branch})$$

("3–1" cluster with single negative charge)

$$\text{negative 3–1 cluster} + Fe \cdot Mg \rightarrow Fe \cdot Mg\text{–}V''Mg\text{–}Fe_I^{\cdot\cdot\cdot}\text{–}V''Mg\text{–}Fe \cdot Mg \quad (V''Mg\text{–}Fe \cdot Mg \text{ branch})$$

(neutral "3–1" cluster)

$$\text{neutral 3–1 cluster} + \text{dimer} \rightarrow \text{4–1 cluster}$$

A set of such units would be consistent with the general details of the Mössbauer spectra, the observed O/T ratio and the coloration, although it is not possible to estimate the relative concentration of individual species.

The $MgO:Fe^{3+}$ samples subjected to a second lower temperature anneal clearly must contain larger clusters owing to the strong coloration. The O/T ratio cannot be obtained with certainty from the Mössbauer measurements owing to the ambiguities in possible fit models, although an O/T ratio smaller than that in the higher temperature sample is indicated. In view of the lattice-energy calculation, the growth of larger clusters should proceed along a spinel motif. The O/T ratio of large magnesioferrite (MF) spinel clusters (size sufficiently great that surface octahedral Fe^{3+} is a small proportion of total Fe^{3+}) approaches 1.5 so that MF cluster growth is consistent with the Mössbauer spectra, although in a qualitative sense.

The O/T Fe^{3+} ratio observed in the 70% Fe magnesiowüstite of 3.0 is consistent with a set of cluster geometries similar to those postulated for the $MgO:Fe^{3+}$ samples. However, because the concentration of Fe^{3+} in these samples is an order of magnitude or more larger than in the doped periclase, it is probable that larger defect clusters exist at equilibrium. This would lead to correspondingly larger clusters in quenched samples. Hence based on the clusters indicated above for quenched $MgO:Fe^{3+}$, 4–1 and larger clusters ought to be present in rapidly quenched magnesiowüstite. In particular, 6–2 or combination of 8–3 and 10–3 units would produce the O/T ratio observed.

Unfortunately, no coloration information can be derived from these uniformly black materials. Also, the Mössbauer spectra are complicated because of the overlap of Fe^{2+} and Fe^{3+} features and the possible presence of averaged valence states due to rapid electron hopping.

In quenched wüstite, there is evidence for clusters of the 8–3 and 10–3 type, which appear to be organized into a large ordered superstructure [29]. Such units would have O/T ratios of 2.33 and 3.67 respectively, producing an average value of about 3.0. Equilibrium studies of wüstite over a range of defect concentrations have suggested 4–1 clusters at low defect levels (O/T = 5) and larger clusters at high defect concentration (O/T = 3) [30, 31].

All of these studies, along with the present work, suggest a similarity of defect clustering throughout the $MgO–Fe_{1-x}O$ system, with the largest single effect being due to Fe^{3+} and cation vacancy concentration. The defect clusters which are stable at equilibrium and which are postulated for rapidly quenched samples are not equivalent to spinel nuclei in either structure or chemistry as judged by both spectroscopic evidence of O/T ratio, X-ray structural information and the lattice-energy calculations which have been performed. Hence a defect cluster reorganization must occur prior to spinel nucleation. In view of the calculated stability of spinel-like units in both the MgO and FeO structure, it is probably such a step which allows quenching-in of any remnants of the equilibrium defect cluster arrangements.

TABLE III MgO–$Fe_{1-x}O$ defect cluster summary

Cluster type	CV/T	Fe^{3+} O/T	Size (Å)	Relative stability (Binding energy/vacancy eV)	
				FeO matrix [7]	MgO matrix [5]
Single tetrahedral 4–1	4.0	5.0	2.2	−1.98	−2.03
2 corner-shared tetrahedra, 7–2	3.5	4.0			
3 corner-shared tetrahedra, 10–3	3.33	3.67			
2 edge-shared tetrahedra, 8–3	3.00	3.00		−2.42	−2.62
4 edge-shared tetrahedra, 10–4	2.50	2.00		−1.90	
Koch–Cohen, 13–4	3.25	3.50	4.4	−2.10	
Inverse spinel, 16–5	3.20	3.40		−2.38	−3.02
Inverse spinel, 25–8	3.125	3.25	8.4		
Inverse spinel 170–64	2.65	2.30	16.8		
Inverse spinel 531–216	2.46	1.91	25.6		
Bulk magnesioferrite	≈ 2.25	≈ 1.50	–		

Acknowledgements

The author is grateful for support during the early part of the investigation from the National Science Foundation grant DES 74-19918 to W. A. Dollase, University of California, Los Angeles. The synchrotron radiation studies were performed at SSRL, which is supported by the NSF through the Division of Materials Research and the NIH through the Biotechnology Resource Program in the Division of Research Resources (in co-operation with the Department of Energy). Reviews of the manuscript by W. A. Dollase, M. Hochella, and J. Pressesky were greatly appreciated.

References

1. U. GONSER, R. W. GRANT, H. WIEDERSICH, R. CHANG and A. H. MUIR, *Bull. Amer. Phys. Co.* **11** (1966) 363.
2. H. R. LEIDER and D. N. PIPKORN, *Phys. Rev.* **165** (1968) 494.
3. B. HENDERSON, J. E. WERTZ, T. P. P. HALL and R. D. DOWSING, *J. Phys.* **C4** (1971) 107.
4. R. A. WEEKS, J. GASTINEQU and E. SONDER, *Phys. Stat. Sol.* **61A** (1980) 265.
5. W. H. GOURDIN and W. D. KINGERY, *J. Mater. Sci.* **14** (1979) 2053.
6. T. A. YAGER and W. D. KINGERY, *ibid.* **16** (1981) 489.
7. C. R. A. CATLOW and B. E. F. FENDER, *J. Phys.* **C8** (1975) 3267.
8. G. A. WAYCHUNAS, Ph.D. Thesis, University of California, Los Angeles (1979).
9. T. A. FINNERTY, G. A. WAYCHUNAS and W. M. THOMAS, *Amer. Mineral.* **63** (1978) 415.
10. E. KANKELEIT, *Rev. Sci. Instrum.* **35** (1964) 194.
11. S. J. H. HUNTER, Ph.D. Thesis, Stanford University (1977).
12. G. S. BROWN and S. DONIACH, "Synchrotron Radiation Research" (Plenum, New York, 1980) Ch. 10, p. 353.
13. S. P. CRAMER, K. O. HODGSON, E. I. STIEFIL and W. E. NEWTON, *J. Amer. Chem. Soc.* **100** (1978) 2748.
14. G. H. VIA, J. H. SINFELT and F. W. LYTLE, *J. Chem. Phys.* **71** (1979) 690.
15. R. D. SHANNON and C. T. PREWITT, *Acta Cryst.* **B25** (1969) 925.
16. I. D. BROWN and R. D. SHANNON, *ibid.* **A29** (1973) 266.
17. R. G. SHULMAN, Y. YAFET, P. EISENBERGER and W. E. BLUMBERG, *Proc. Nat. Acad. Sci. USA* **73** (1975) 1384.
18. G. A. WAYCHUNAS, M. J. APTED and G. E. BROWN, *Phys. Chem. Miner.* submitted.
19. H. H. WICKMAN, *Mössbauer Effect Methodology* **2** (1966) 39.
20. E. DE GRAVE, A. GOVAERT, D. CHAMBAERE and G. ROBBRECHT, *Physica* **96B** (1979) 103.
21. G. A. SAWATZKY, F. VAN DER WOUDE and A. H. MORRISH, *Phys. Rev.* **183** (1969) 383.
22. R. INGALLS, *ibid.* **122** (1964) A787.
23. S. L. RUBY, *Mössbauer Effect Methodology* **8** (1973) 263.
24. G. R. ROSSMAN, personal communication (1980).
25. *Idem, Amer. Mineral.* **60** (1975) 698.
26. W. KUNDIG, H. BOMMEL, G. CONSTABARIS and R. H. LINDQUIST, *Phys. Rev.* **142** (1966) 327.
27. C. J. KRIESMAN and S. E. HARRISON, *ibid.* **103** (1956) 857.
28. R. PAUTHENET and L. BOCHIROL, *J. Phys. Radium* **12** (1951) 249.

29. B. ANDERSON and J. O. SLETNES, *ibid.* **A33** (1977) 268.
30. F. KOCH and J. B. COHEN, *Acta Cryst.* **B25** (1969) 275.
31. A. K. CHEETHAM, B. E. F. FENDER and R. I. TAYLOR, *J. Phys.* **C4** (1971) 2160.

Received 22 February
and accepted 28 June 1982